

Combustion Theory and Modelling



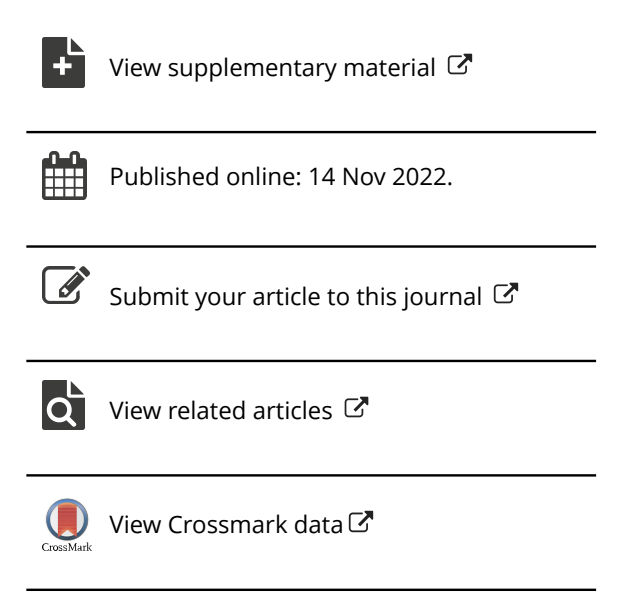
ISSN: (Print) (Online) Journal homepage: https://www.tandfonline.com/loi/tctm20

PeleLM-FDF large eddy simulator of turbulent reacting flows

Aidyn Aitzhan, Shervin Sammak, Peyman Givi & Arash G. Nouri

To cite this article: Aidyn Aitzhan, Shervin Sammak, Peyman Givi & Arash G. Nouri (2022): PeleLM-FDF large eddy simulator of turbulent reacting flows, Combustion Theory and Modelling, DOI: <u>10.1080/13647830.2022.2142673</u>

To link to this article: https://doi.org/10.1080/13647830.2022.2142673







PeleLM-FDF large eddy simulator of turbulent reacting flows

Aidyn Aitzhan ¹⁰a*, Shervin Sammak ¹⁰a,b, Peyman Givi ¹⁰a and Arash G. Nouri ¹⁰a

^aMechanical Engineering and Materials Science, University of Pittsburgh, Pittsburgh, PA, USA

^bCenter for Research Computing University of Pittsburgh, Pittsburgh, PA, USA

(Received 17 January 2022; accepted 10 October 2022)

A new computational methodology, termed 'PeleLM-FDF' is developed and utilised for high fidelity large eddy simulation (LES) of complex turbulent combustion systems. This methodology is constructed via a hybrid scheme combining the Eulerian PeleLM base flow solver with the Lagrangian Monte Carlo simulator of the filtered density function (FDF) for the subgrid scale reactive scalars. The resulting methodology is capable of simulating some of the most intricate physics of complex turbulence-combustion interactions. This is demonstrated by LES of a non-premixed CO/H₂ temporally evolving jet flame. The chemistry is modelled via a skeletal kinetics model, and the results are appraised via *a posteriori* comparisons against direct numerical simulation (DNS) data of the same flame. Excellent agreements are observed for the time evolution of various statistics of the thermo-chemical quantities, including the manifolds of the multi-scalar mixing. The new methodology is capable of capturing the complex phenomena of flame-extinction and re-ignition at a 1/512 of the computational cost of the DNS. The high fidelity and the computational affordability of the new PeleLM-FDF solver warrants its consideration for LES of practical turbulent combustion systems.

Keywords: large eddy simulation; turbulent combustion; filtered density function; low mach number approximation

1. Introduction

Since its original proof of concept [1, 2], the filtered density function (FDF) has become very popular for large eddy simulation (LES) of turbulent flows. This popularity is due to an inherent capability of the FDF to account full statistics of the subgrid scale (SGS) quantities; and thus it is more accurate than conventional SGS models which are based on low order SGS moments. This superior performance comes at a price. The FDF transport equation is somewhat more difficult and computationally more expensive to solve, as compared to traditional LES schemes. The last decade has witnessed significant progress in improvement and popularity of FDF as evidenced by a rather large number of publications; *e.g.* Refs. [3–29]. Parallel with these developments, there have also been extensive studies regarding the FDF accuracy & reliability [16, 22, 30–33], and sensitivity analysis of its simulated results [34, 35]. For comprehensive reviews of progress within the last decade, see Refs. [36, 37].

Despite the remarkable progress as noted, there is still a continuing demand for further improvements of LES-FDF for prediction of complex turbulent combustion systems. In particular, it is desirable to develop FDF tools which are of high fidelity, and are also

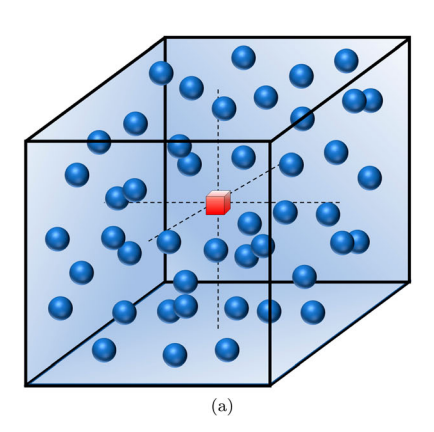
^{*}Corresponding author. Email: aia29@pitt.edu

computationally affordable. In the present work, the PeleLM [38] base flow solver is combined with the parallel Monte Carlo FDF simulator [4, 39] in a hybrid manner that takes full advantage of modern developments in both strategies. PeleLM is a massively parallel simulator of reactive flows at low Mach numbers. These flows are of significant interest in several industries such as gas turbines, IC engines, furnaces and others. The solver is based on block-structured AMR algorithm [40] through the AMReX numerical software library [41] (formerly called BoxLib [42]). This solver uses a variable density projection method [43-45] for solving three-dimensional Navier-Stokes and reaction-diffusion equations. The computational discretization is based on structured finite volume (FV) for spatial discretization, and a modified spectral deferred correction (SDC) algorithm [46-49] for temporal integration. The solver is capable of dealing with complex geometries via the embedded boundary method [50, 51], and runs on modern platforms for parallel computing such as MPI + OpenMP for CPUs and MPI + CUDA or MPI + HIP for GPUs. The fidelity of PeleLM has been demonstrated to be effective for DNS of a variety of reactive turbulent flows [52-56]. Here, the PeleLM is augmented to include LES capabilities by hybridising it with the FDF-SGS closure. The resulting solver is shown to be computationally efficient, and to produce results consistent with those generated by high-fidelity, and much more expensive DNS.

2. Hybrid PeleLM-FDF solver

Formulation is based on the variable density turbulent reacting flow involving N_s species in which the flow velocity is much less than the speed of sound [2, 57]. In this flow, the primary transport variables are the fluid density $\rho(x,t)$, the velocity components $u_i(x,t)$, i=1,2,3 along the x_i direction, the specific enthalpy h(x,t), the pressure p(x,t), and the species mass fractions $Y_{\alpha}(x,t)$ ($\alpha=1,2,\ldots,N_s$). The conservation equations governing these variables are the continuity, momentum, enthalpy (energy) and species mass fraction equations, along with an equation of state [58]. Large eddy simulation involves the use of the spatial filtering operation, with $\langle Q(\mathbf{x},t)\rangle_{\ell}$ denoting the filtered value of the transport variable $Q(\mathbf{x},t)$ and $\langle Q(\mathbf{x},t)\rangle_L = \langle \rho Q \rangle_\ell / \langle \rho \rangle_\ell$ representing its density weighted (Favre) average. The FDF of only the scalar variables are considered. In the FDF transport equation, the effects of the subgrid scale (SGS) convection are modelled by the standard gradient diffusion model [59, 60] with the Vreman's model [61] for the SGS viscosity, and unity SGS Prandtl and Schmidt numbers. The influence of SGS mixing is taken into account with the LMSE/IEM closure [62]. Modelled stochastic differential equations are constructed to portray these models. These SDEs are solved via a Lagrangian Monte Carlo (MC) routine [57].

AMReX library is a very powerful computational software with many useful functions, templates, and classes including linear solvers [63] and particle containers [64]. The latter is especially useful for our purpose. The principal algorithm is based on a variable density projection method for low Mach number flows as described in Ref. [65]. The domain is discretised by an ensemble of finite volume cells and the particles are free to move within the domain (Figure 1). The MC procedure is implemented by deriving a new class from the particle container of the AMReX library, adding all the required functions including procedures for grid-to-particle interpolation, particle SDE & ODE solving and ensemble averaging. The particles' transport is simulated via the Euler-Maruyama scheme [66], and the compositional makeup is updated with a third order Runge-Kutta solver.



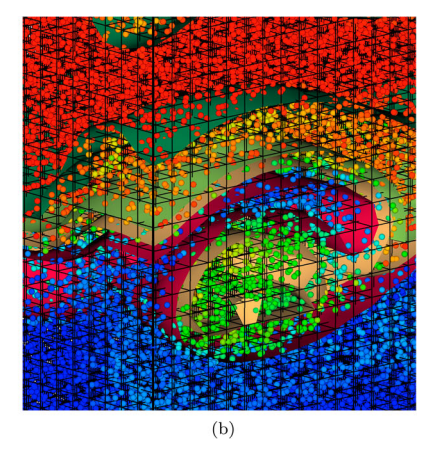


Figure 1. (a) Ensemble averaging in MC simulations. The red cube denotes the finite volume cell centre, and the blue spheres denote the MC particles. (b) Example of MC particles within the Eulerian field identified by PeleLM. The colours of the MC particles provide a measure of the particle's scalar values.

The filtered density, all of the mass fractions, and the enthalpy can be evaluated via both PeleLM ad the MC-FDF solvers. The filtered chemical source term can be evaluated only by via MC-FDF. This is done by conducting ensemble averaging involving N_E elements within a volume of $(\Delta_E)^3$ at the points of interest. The consistency of the hybrid solver is assessed by instantaneous comparison of the filtered variables simulated by the two solvers. The consistency of the density field, in particular, is assessed by the scheme devised in previous work [57]. The choice of Δ_E is independent of the grid size Δx , and the LES filter size Δ_G . It is desirable to set Δ_E as small as possible. The particle-grid interaction is schematically illustrated in Figure 1(a), while the example of an actual hybrid Eulerian-Lagrangian simulation is shown in Figure 1(b). The transfer of information from the grid points to the MC particles is accomplished via a linear interpolation. Higher accuracy can be achieved by constructing the MC averages via linear weighting [67] and/or adaptive cloning of the MC particles [25, 68]. The computational procedure is summarised via Algorithm ??. The algorithm shows the steps involved in a single time-advancements from time level n to n + 1. Steps 1, 5 and 6 are from the original Pelel-LM. Steps 2-4 are the FDF-MC inserts. Of primary importance is Step 4 in which the filtered chemical source term is determined. This term is subsequently utilised in Step 5 to update the scalar fields. Time advancement is completed in Step 6 where the velocity-pressure coupling is finalised. Step 7 is solely for the purpose of accuracy assurance, and is recommended in all hybdrid Eulerian-Lagrangian solvers [57].

3. Flow configuration and model specifications

The performance of the PeleLM-FDF solver is assessed by conducting LES of a temporally evolving planar turbulent CO/H_2 jet flame. This flame has been the subject of detailed DNS [69], and several subsequent modelling and simulations [70–75]. The flame is rich with strong flame—turbulence interactions resulting in local extinction followed by re-ignition. The flow configuration is the same as that considered in DNS and is depicted in Figure 2. The jet consists of a central fuel stream of width H surrounded by counter-flowing

Algorithm 1 Hybrid PeleLM-FDF Algorithm

- 1: Advance the velocity field from time-level n to level n + 1/2 via PeleLM.
- 2: Interpolate the relevant variables from the fixed Eulerian points to the instantaneous particle locations.
- 3: Integrate the modelled SDEs describing the MC-transport and ODEs describing species' compositional setup.
- 4: Construct the filtered values of all of the scalars $\langle \phi \rangle_{L,MC}^{n+1}$, the density $\langle \rho \rangle_{\ell,MC}^{n+1}$, and the chemical source terms $\langle \mathbf{S} \rangle_{L,MC}^{n+1}$ from the MC field.
- 5: Advance the scalars field and the density via the PeleLM.
- 6: Evaluate the pressure and update the velocity field at level n + 1.
- 7: Conduct consistency assessments by comparisons of the scalars fields and he density as obtained via the PeleLM and MC-FDF.

oxidiser streams. The fuel stream is comprised of 50% of CO, 10% H_2 and 40% N_2 by volume, while oxidiser streams contain 75% N_2 and 25% O_2 . The initial temperature of both streams is 500 K and thermodynamic pressure is set to 1 atm. The velocity difference between the two streams is $U = 276 \,\mathrm{m/s}$. The fuel stream velocity and the oxidiser stream velocity are U/2 and -U/2, respectively. The Reynolds number, based on U and H is Re = 9, 079. The sound speeds in the fuel and oxidiser streams denoted as C_1 and C_2 , respectively and the Mach number $Ma = U/(C_1 + C_2) = 0.3$ is small enough to justify a low Mach number approximation. The combustion chemistry is modelled via the skeletal kinetics, containing 11 species with 21 reaction steps [69]. The initial conditions are taken directly from DNS. The boundary conditions are periodic in stream wise (x) and spanwise (z) directions, and the outflow boundary conditions imposed at $y = \pm L_y/2$. The FDF simulations are conducted in the same as those in previous LES-FDF [39].

The size of the computational domain is $L_x \times L_y \times L_z = 12H \times 14H \times 8H$. The time is normalised by $t_j = H/U$. The domain is discretised into equally spaced structured fixed grids of size $N_x \times N_y \times N_z = 108 \times 126 \times 72$. The resolution, as selected, is the largest that was conveniently available to us, and kept the SGS energy within the allowable $15\% \sim 20\%$ of the total energy. This resolution should be compared with $N_{x,DNS} \times N_{y,DNS} \times N_{z,DNS} = 864 \times 1008 \times 576$ grids as utilised in DNS [69]. The sizes of the ensemble domain, the subgrid filter and the finite volume cells are taken to be equal $\Delta_E = \Delta_G = \Delta x = \Delta y = \Delta z = L_x/N_x$, and the timestep for temporal integration is $\Delta t = 10^{-7}$ s. The number of MC particles per grid point is set to 64; so there are over 62.7 million MC particles portraying the FDF at all time. With a factor of 512 times smaller number of grid points, the total computational time for the simulations is around 400 CPU hours on 2 nodes of 28-core Intel Xeon E5-2690 2.60 GHz (Broadwell) totalling 56 processors.

The simulated results are analysed both instantaneously and statistically. In the former, the instantaneous contours (snap-shots) and the scatter plots of the reactive scalar fields are considered. This pertains to the temperature and mass fractions of all of the species. In the latter, the 'Reynolds-averaged' statistics are constructed. With the assumption of a temporally developing layer, the flow is homogeneous in the z- and the x- directions. Therefore, all of the Reynolds averaged values, denoted by an overline, are temporally evolving and determined by ensemble averaging over the x-z planes. The resolved stresses are denoted by $R(a,b) = \overline{\langle a \rangle_L \langle b \rangle_L} - \overline{\langle \langle a \rangle_L \rangle}$, and the total stresses

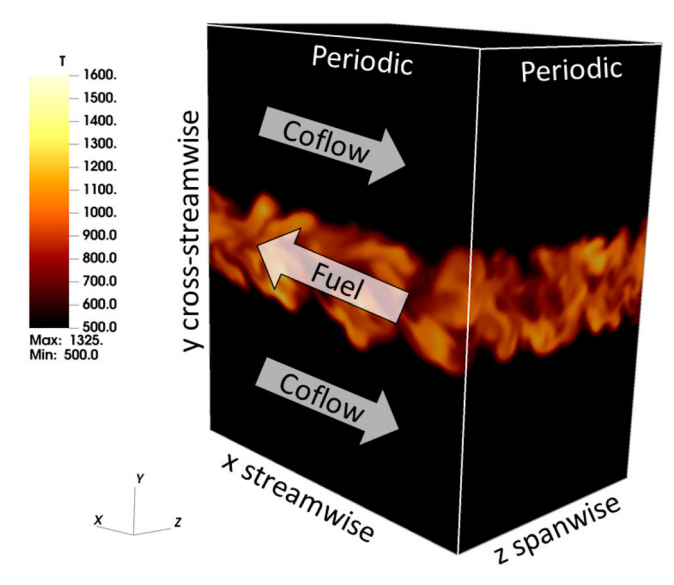


Figure 2. Schematics of the temporally developing turbulent jet flame. The jet consists of a central fuel stream surrounded by two counter-flowing oxidiser streams. The fuel stream is comprised of 50% of CO, 10% H₂ and 40% N₂ by volume, while oxidiser streams contain 75% N₂ and 25% O₂. The initial temperature of both streams is 500 K and the thermodynamic pressure is set to 1 atm.

are denoted by $r(a,b) = \overline{(ab)} - \overline{ab}$. The latter can be evaluated directly from the fine-grid DNS data $r_{\text{DNS}}(a,b)$. In LES with the assumption of a generic filter, i.e. $\overline{\langle Q \rangle_L} = \overline{Q}$, the total stresses are approximated by $r_{\text{LES}}(a,b) = R(a,b) + \overline{\tau(a,b)}$ [76, 77], where $\tau(a,b)$ is the subgrid variance. The root mean square (RMS) values are square roots of these stresses. To analyse the compositional flame structure, the 'mixture fraction' field $Z(\mathbf{x},t)$ is also constructed. Bilger's formulation [78, 79] is employed for this purpose.

4. Presentation of results

For the purpose of flow visualisation, the contour plots of the temperature field are presented in Figure 3 for several consecutive time-instances. These contours show the formation of structures within the flow, and the growth of the layer from the initial perturbed laminar to a highly three-dimensional turbulent flow. To demonstrate the consistency, comparisons are made between the filtered values as obtained by the Lagrangian and Eulerian simulators. Figure 4 shows the instantaneous scatter plots of the temperature and mixture fraction, and Figure 5 shows the Reynolds averaged values of these variables. The correlation coefficients between the averaged MC and FV scattered for both the temperature and the mixture fraction fields are greater than 0.99 at all time instances, and the Reynolds averaged results are indistinguishable. This level of consistency is observed throughout the entire simulations.

The fidelity of LES predictions are assessed via comparisons with DNS. This is shown for the first and second Reynolds-moments of the mixture fraction, the temperature, and the mass fractions of major species (CO, CO₂) at several time steps in Figure 6. Additionally, 2D slice plots of LES-FDF and DNS are shown in Figure 7 for a more detailed view. In all of these cases, the DNS captures more of the small scale features which are filtered

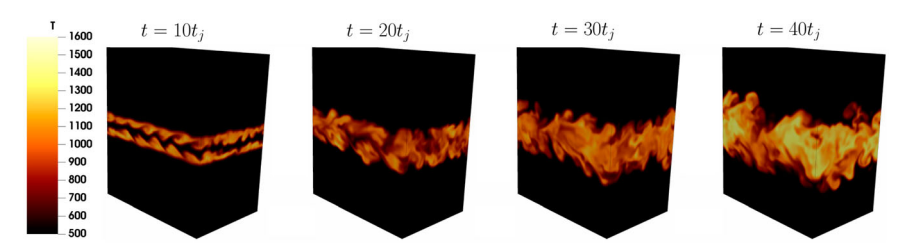


Figure 3. Temporal evolution of the temperature field.

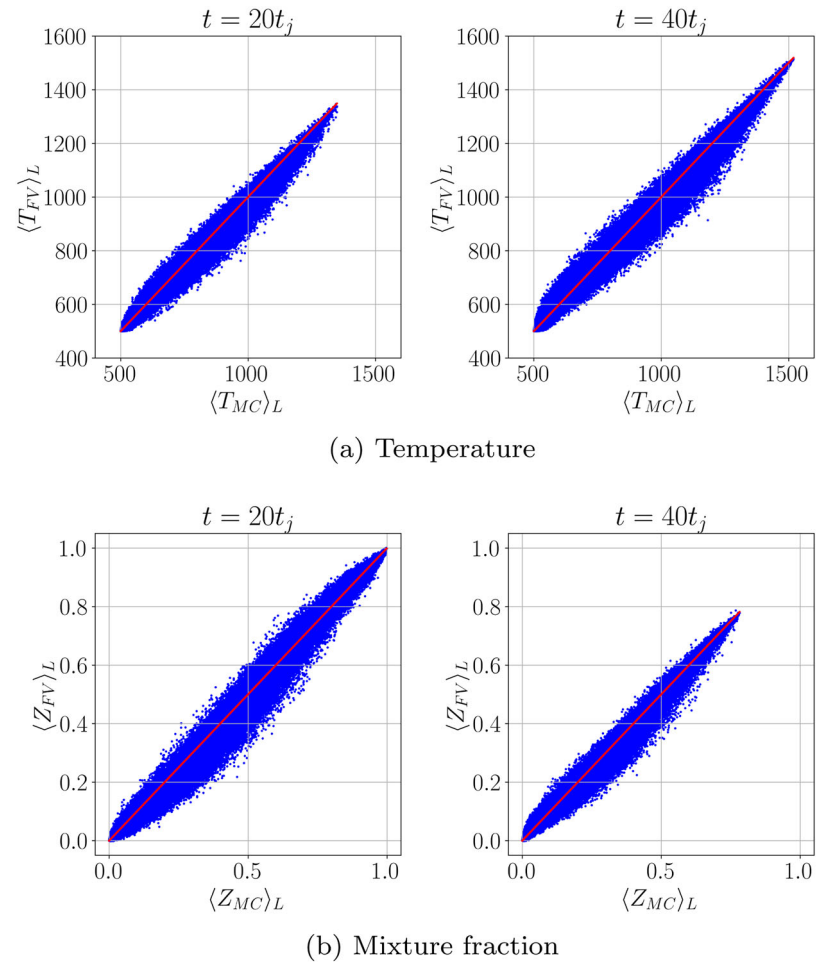


Figure 4. Scatter plots of the Eulerian vs. the Lagrangian filtered values. (a) Temperature (b) Mixture fraction.

out by LES. Therefore, the spreading rate as predicted by LES is somewhat larger than that in DNS. The initial decrease of the temperature at $t \approx 20t_j$ is an indication of flame extinction, and its increase at later times ($t \approx 40t_j$) signals re-ignition.

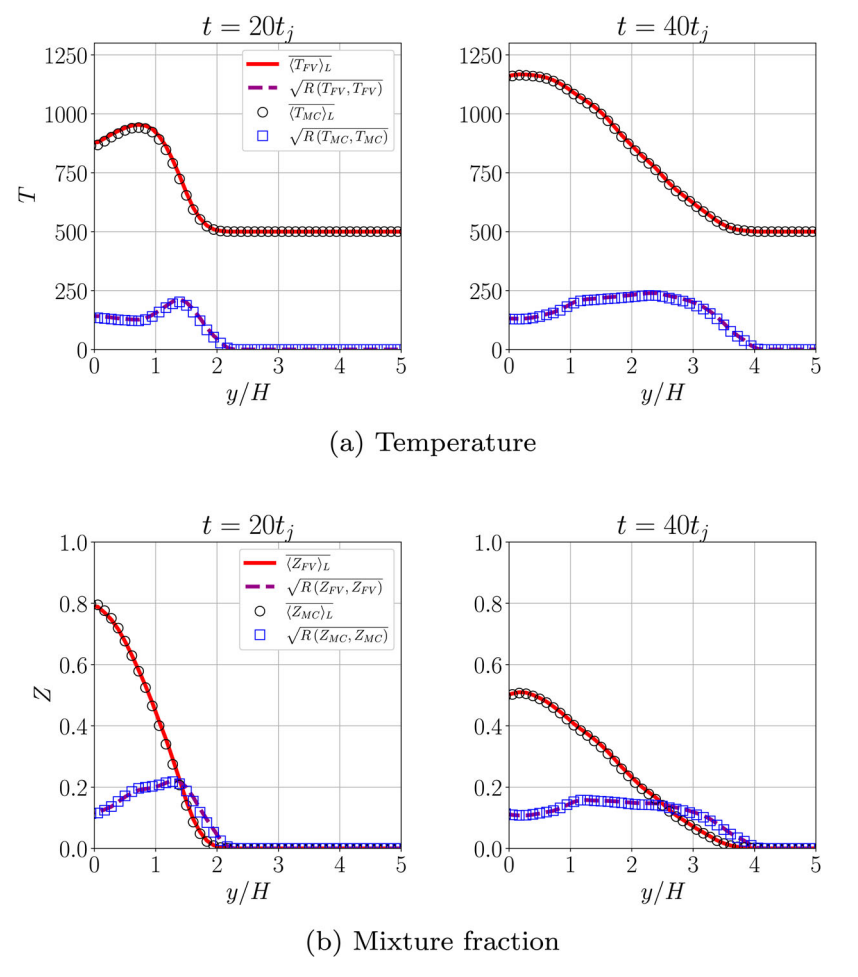


Figure 5. Reynolds-averaged Eulerian (lines) vs. the Lagrangian filtered (symbols) values in the cross-stream direction. (a) Temperature (b) Mixture fraction.

As an evidence of overall layer growth, the mixture fraction thickness is constructed. This thickness is defined as $\delta_Z = 2$ arg min $(|\overline{Z}(y) - \epsilon|)$ for y > 0, where ϵ is a small positive number. The temporal evolution of this thickness, shown in Figure 8, indicates that the growth of a turbulent layer predicted by LES is close to that obtained by DNS at initial times. However, as the flow develops the LES predicts a larger rate of spreading for the layer. This is most likely due to inadequacies of the simple gradient diffusion model for the SGS convection, as demonstrated in previous work [80].

The flame extinction phenomenon and its subsequent re-ignition is explained in terms of the dissipation of the mixture fraction: $\chi = 2\gamma/\rho \nabla Z \cdot \nabla Z$ [79, 81], where γ denotes the thermal diffusivity coefficient. The Reynolds-averaged values of this dissipation, implicitly modelled here as: $\langle \chi \rangle_L = 2\Omega \tau(Z,Z)$ are shown in Figure 9. Here Ω is the subgrid mixing frequency and $\tau(Z,Z)$ is the subgrid variance of the mixture fraction. All of the predicted results agree very well with DNS measured data. At initial times, when the dissipation rates are large, the flame cannot be sustained and is locally extinguished. At later

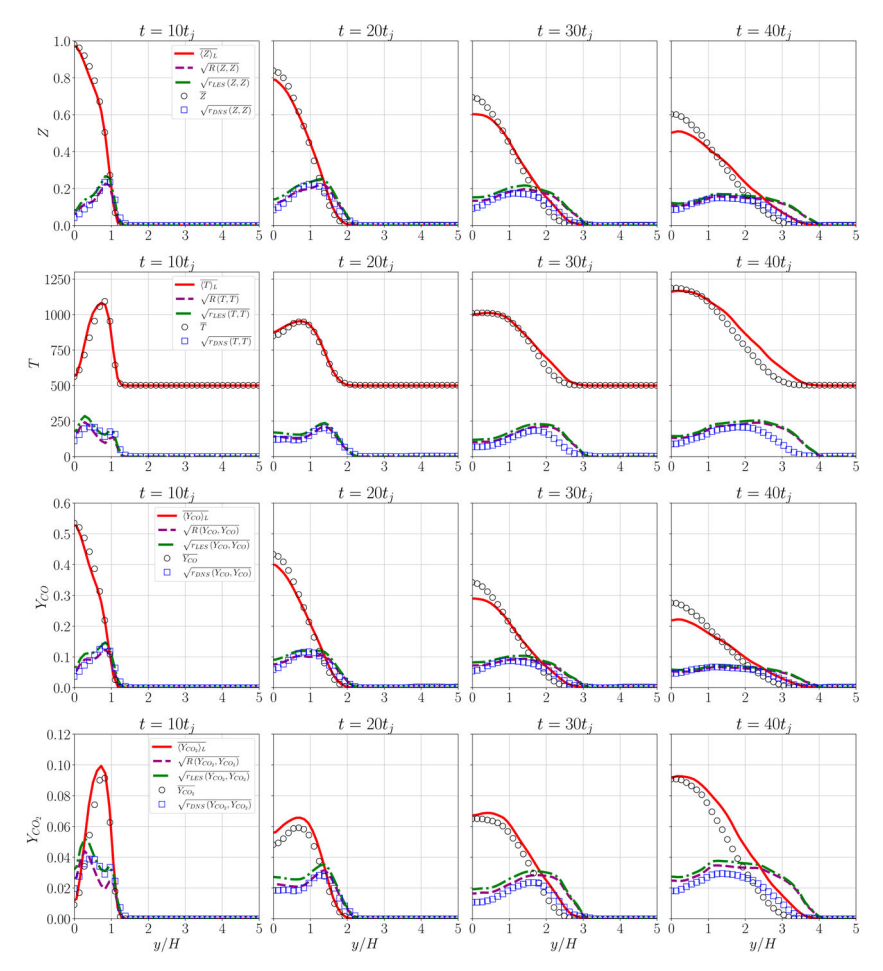


Figure 6. Reynolds-averaged mean and RMS values of the mixture fraction (Z), temperature (T), CO mass fraction (Y_{CO_2}), and CO₂ mass fraction (Y_{CO_2}). Lines and symbols denote LES and DNS results, respectively.

times, when the dissipation values are lowered, the flame is re-ignited and the temperature increases. This dynamic is more clearly depicted in Figure 10, where the expected temperature values conditioned on the mixture fraction are shown. By $t = 20t_j$ the temperature at the stoichimetric mixture fraction ($Z_{st} = 0.42$) decreases from T = 1400 K, stays below extinction limit for a while, and then rises after $t = 30t_j$. The agreement with DNS data for this conditional expected value is very good.

To provide a more quantitative assessment of the flame structure within the entire domain, an 'extinction marker' is defined as $M_{ext} = (H(Y_{OH} - Y_{OH,c}) \mid Z = Z_{st})$ [82]. Here, $Y_{OH,c} = 0.0007$ is a cut-off mass fraction of hydroxyl radical and H(x) denotes the Heaviside function. (A video-clip is provided in Supplementary Materials.) The volume averaged extinction marker defines the probability of a point experiencing extinction: $\frac{1}{V} \int_V M_{ext} \, \mathrm{d}V = P(Z = Z_{st}, Y_{OH} \le Y_{OH,c})$ and its evolution over time is shown in Figure 11(a). The excellent agreement between LES and DNS on the figure indicates

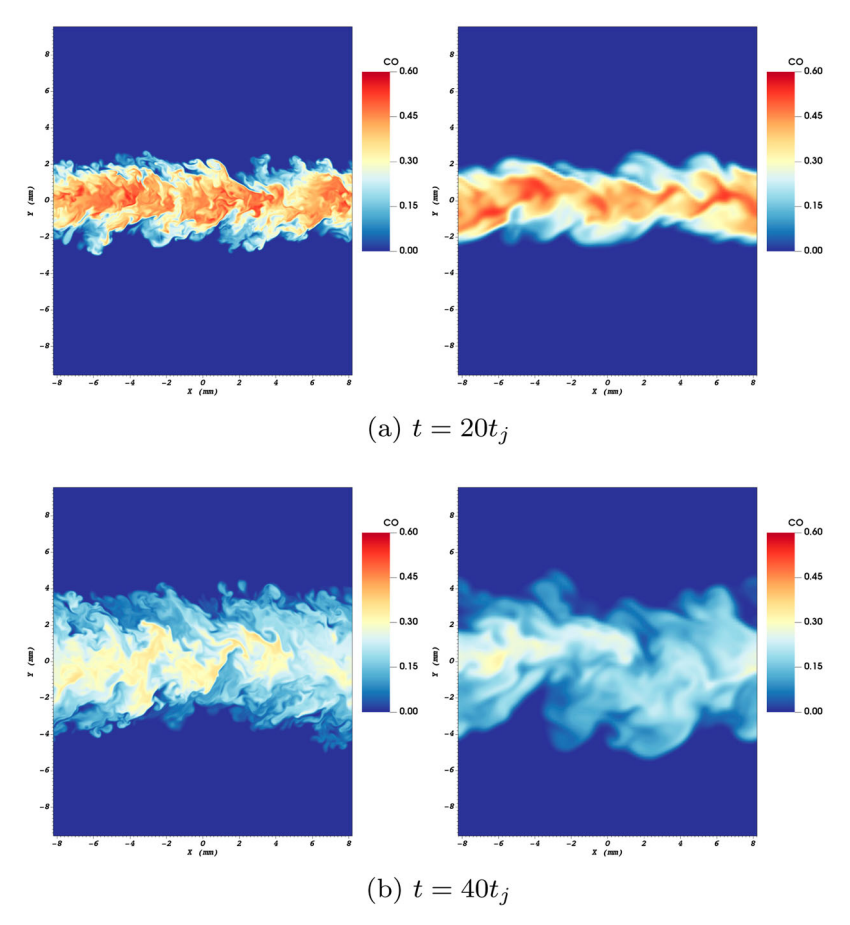


Figure 7. Instantaneous slice plots at z=0 of CO mass fraction obtained from DNS (left) and LES-FDF (right). (a) $t=20t_j$ (b) $t=40t_j$.

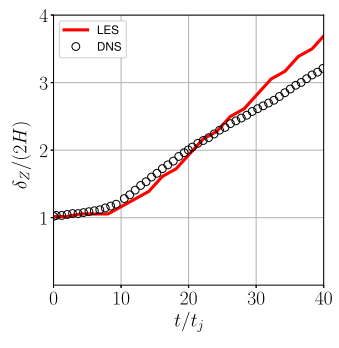


Figure 8. Temporal evolution of mixture fraction thickness. Lines and symbols denote the LES and DNS values, respectively.

that the timings of extinction and re-ignition as predicted by LES are accurate. The temporal evolution of the expected temperature conditioned on the stoichiometric mixture fraction in Figure 11(b) corroborates the onset of extinction due to high dissipation and

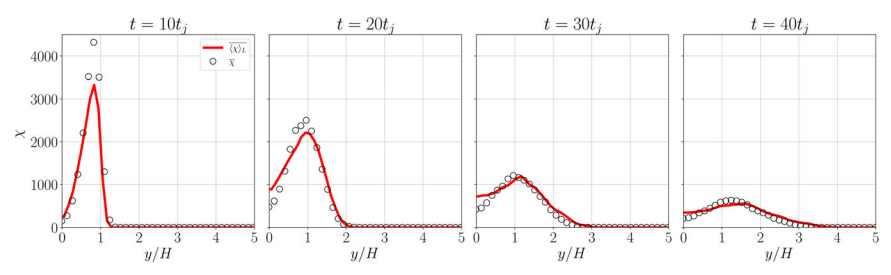


Figure 9. Reynolds-averaged values of scalar dissipation rate. Lines and symbols denote the LES and DNS values, respectively.

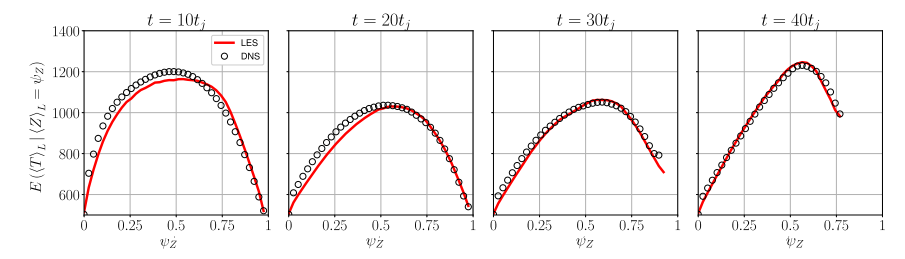


Figure 10. Volume averaged temperature conditioned on mixture fraction. Lines and symbols denote the LES and DNS values, respectively.

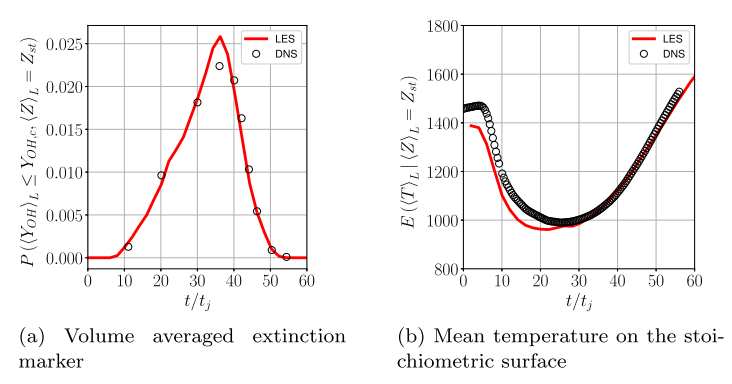


Figure 11. Temporal evolution of average extinction and re-ignition. Lines and symbols denote the LES and DNS values, respectively. (a) Volume averaged extinction marker (b) Mean temperature on the stoichiometric surface.

the subsequent re-ignition at low dissipation. The increase of temperature at final times is accompanied by Y_{CO2} production and Y_{CO} consumption at later times, as observed in Figure 6.

A more comprehensive comparison with DNS is done by examination of the mixture fraction PDFs in Figure 12. In DNS these PDF generated by sampling of $N_{x,DNS} \times 8 \times N_{z,DNS}$ near the centre-plane ($|y| < \Delta y$) of the jet (8 cross-stream planes). The LES generated PDFs are based on sampling of $N_x \times 2 \times N_z$ (2 cross-stream planes). While the two sets of PDFs are qualitatively the same, there are some small quantitative differences. The DNS generated PDFs tend to be concentrated near the higher mixture fraction values. This is consistent with the observations made in Figure 6, indicating a higher jet spreading rate

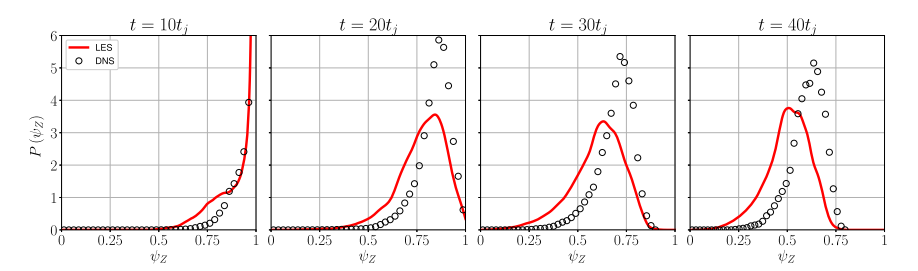


Figure 12. Probability density function of mixture fraction about y = 0 plane. Lines and symbols denote the LES and DNS values, respectively.

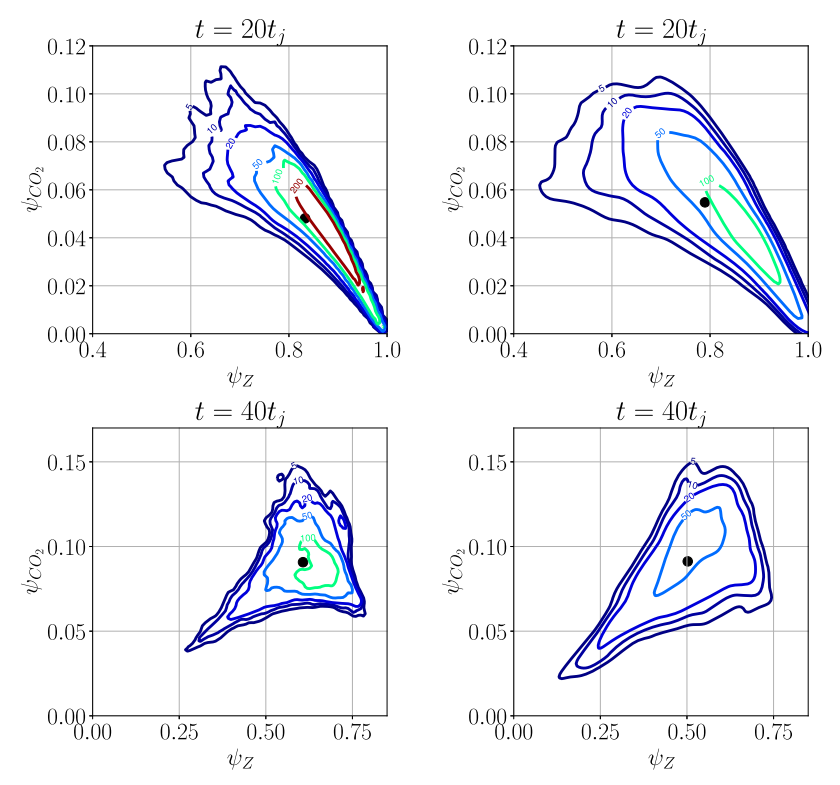


Figure 13. Joint probability density functions of mixture fraction and Y_{CO_2} about y = 0 plane of DNS (left) and LES (right).

in LES. However, the width of the PDFs are the same, consistent with the RMS values shown in Figure 6. To portray the dynamics of multi-scalar mixing and reaction, the joint PDFs of the scalar variables must be considered. The mixture fraction and the mass fraction of the CO_2 are considered, and the results are shown in Figure 13. In both cases, as the flow becomes fully turbulent at $t = 40t_j$, the PDFs tend to have a multi-variate Gaussian distribution. In all cases, the LES predicted PDFs are in excellent agreement with those depicted by DNS. Finally, to asses the LES predictions of the overall compositional structure, three-dimensional scatter plots of the mixture fraction, the mass fraction of oxidant O_2 and the mass fraction of hydroxyl radical OH coloured by temperature are shown in

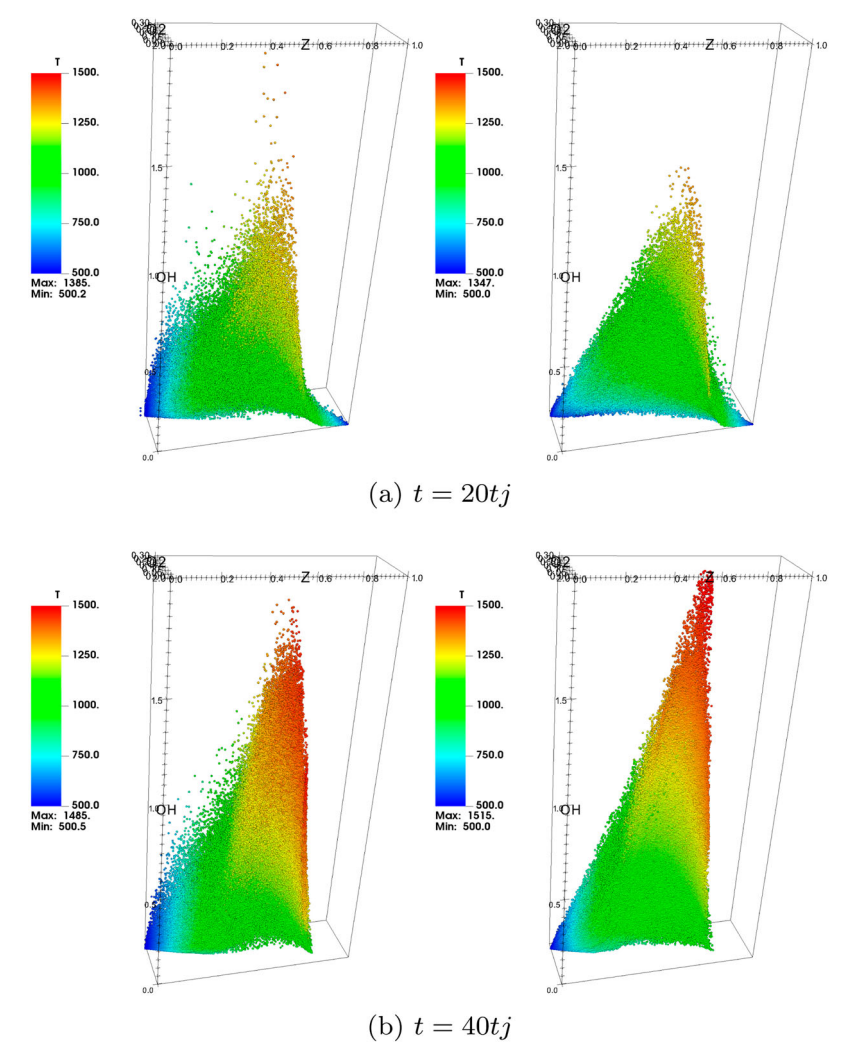


Figure 14. Scatter plot of mixture fraction Z, oxidant mass fraction Y_{O_2} , and hydroxyl radical mass fraction $Y_{OH} \times 1000$ coloured by temperature of DNS (left) and LES (right). (a) t = 20tj (b) t = 40tj.

Figure 14. Again, the manifolds as predicted by LES-FDF are in very good agreements with those depicted by DNS.

5. Conclusions

Modeling of turbulence-combustion interactions has been the subject of broad investigations for over seventy years now [83]. Large eddy simulation has been long recognised as a convenient means of capturing the unsteady evolution of turbulence in both non-reacting and reactive flows [84]. The major issues associated with LES for prediction of practical turbulent combustion problems are: reliable modelling of SGS quantities, high fidelity solution of the modelled transport equations, and versatility in dealing with

complex flames. The filtered density function [36, 85–88] has proven particularly effective in resolving the first issue. The present work makes a progress in dealing with the other two. This progress is facilitated by developing a novel computational scheme by the merger of the PeleLM flow solver [48, 49, 65] and the Monte-Carlo (FDF) simulator. The resulting computational scheme facilitates reliable and high fidelity simulation of turbulent combustion systems. The novelty of the methodology, as developed, is its capability to capture the very intricate dynamics of turbulence-chemistry interactions. This is demonstrated by its implementation to conduct LES of a CO/H₂ temporally developing jet flame. The results are assessed via detailed a posteriori comparative assessments against DNS data for the same flame [69]. Excellent agreements are observed for the temporal evolution of all of the thermo-chemical variables, including the manifolds portraying the multi-scalar mixing. The new methodology is shown to be particularly effective in capturing non-equilibrium turbulence-chemistry interactions. This is demonstrated by capturing the flame-extinction and its re-ignition as observed in DNS. With its high fidelity and computational affordability, the new PeleLM-FDF simulator as developed here provides an excellent tool for computational simulations of complex turbulent combustion systems.

At this point it is instructive to provide some suggestions for future works in continuation of this research:

- (1) The hydrodynamic SGS closure adopted here is based on the zero-order model of Vreman [61]. This model has proven very effective for LES of many flows, including the one considered here. However, for more complex flows one may need to use more comprehensive SGS closures. Therefore, the extension to include the velocity-FDF [80, 89–91] is encouraged.
- (2) A very attractive feature of the PeleLM is its adaptive gridding and mesh refinement strategy. This feature is not utilised here because of the relative flow simplicity. Future work is needed to refine the MC strategy in conjunction with AMR. Some progress in this regard has been reported [6, 8].
- (3) The FDF-MC has experienced continual upgrades within the past decade [36]. As examples: sparse-Lagrangian MC for better performance with small number of particles [7, 32, 92], high order SDE solver for more accurate particle integration [93], mass consistency assurance [94], spline-averaging of the MC particles for higher order calculations of the moments [30]. These upgrades can be implemented into future versions of the present hybrid simulator.
- (4) The PeleC code [95] is the counterpart of PeleLM for high speed flows. It would be desirable to implement the FDF methodology in this code as well. In doing so, the full self-contained form of the FDF [18] should be considered.
- (5) Resolution assessment in LES is of crucial importance. Several such studies have been conducted for other forms of LES-FDF [16, 21, 96], and is recommended for PeleLM-FDF.
- (6) With its flexibility and high fidelity, it is expected that the PeleLM-FDF methodology will be implemented for LES of a wide variety of other complex turbulent combustion systems.

Acknowledgments

We are grateful to Professor Evatt R. Hawkes of the University of New South Wales for providing the DNS data as used for comparative studies here. We are indebted to Dr. Marcus Day of National Renewable Energy Laboratory, the original developer of the PeleLM for excellent comments on the

draft of this manuscript. Computational resources are provided by the University of Pittsburgh Center for Research Computing.

Disclosure statement

No potential conflict of interest was reported by the author(s).

Funding

This work is sponsored by the National Science Foundation [grant numbers CBET-2042918 and CBET-2152803].

ORCID

Aidyn Aitzhan http://orcid.org/0000-0001-9524-8989

Shervin Sammak http://orcid.org/0000-0003-0796-1886

Peyman Givi http://orcid.org/0000-0002-9557-5768

Arash G Nouri http://orcid.org/0000-0001-7390-5212

References

- [1] Colucci P.J., Jaberi F.A., Givi P., and Pope S.B., Filtered density function for large eddy simulation of turbulent reacting flows, Phys. Fluids 10 (1998), pp. 499–515.
- [2] Jaberi F.A., Colucci P.J., James S., Givi P., and Pope S.B., Filtered mass density function for large-eddy simulation of turbulent reacting flows, J. Fluid Mech. 401 (1999), pp. 85–121.
- [3] Ansari N., Goldin G.M., Sheikhi M.R.H., and Givi P., Filtered density function simulator on unstructured meshes, J. Comput. Phys. 230 (2011), pp. 7132–7150.
- [4] Ansari N., Pisciuneri P.H., Strakey P.A., and Givi P., Scalar-filtered mass-density-function simulation of swirling reacting flows on unstructured grids, AIAA J. 50 (2012), pp. 2476–2482.
- [5] Ansari N., Strakey P.A., Goldin G.M., and Givi P., Filtered density function simulation of a realistic swirled combustor, Proc. Combust. Inst. 35 (2015), pp. 1433–1442.
- [6] Castro L.P., Pinheiro A.P., Vilela V., Magalhães G.M., Serfaty R., and Vedovotto J.M., Implementation of a hybrid Lagrangian filtered density function-large eddy simulation methodology in a dynamic adaptive mesh refinement environment, Phys. Fluids 33 (2021), p. 045126.
- [7] Cleary M.J., Klimenko A.Y., Janicka J., and Pfitzner M., A sparse-Lagrangian multiple mapping conditioning model for turbulent diffusion flames, Proc. Combust. Inst. 32 (2009), pp. 1499– 1507.
- [8] Damasceno M.M.R., de Freitas Santos J.G., and Vedovoto J.M., Simulation of turbulent reactive flows using a FDF methodology advances in particle density control for normalized variables, Comput. Fluids 170 (2018), pp. 128–140.
- [9] de Almeida Y.P. and Navarro-Martinez S., Large eddy simulation of a supersonic lifted flame using the Eulerian stochastic fields method, Proc. Combust. Inst. 37 (2019), pp. 3693–3701.
- [10] Inkarbekov M., Aitzhan A., Kaltayev A., and Sammak S., A GPU-accelerated filtered density function simulator of turbulent reacting flows, Int. J. Comput. Fluid Dyn. 34 (2020), pp. 381– 396.
- [11] Komperda J., Ghiasi Z., Li D., Peyvan A., Jaberi F., and Mashayek F., A hybrid discontinuous spectral element method and filtered mass density function solver for turbulent reacting flows, Numer. Heat Transfer, Part B 78 (2020), pp. 1–29.
- [12] Mejía J.M., Chejne F., Molina A., and Sadiki A., Scalar mixing study at high-schmidt regime in a turbulent jet flow using large-eddy simulation/filtered density function approach, J. Fluids Eng. 138 (2016), p. 021205.
- [13] Minier J., Chibbaro S., and Pope S.B., Guidelines for the formulation of Lagrangian stochastic models for particle simulations of single-phase and dispersed two-phase turbulent flows, Phys. Fluids 26 (2014), p. 113303.

- [14] Natarajan H., Popov P., and Jacobs G., A high-order semi-Lagrangian method for the consistent Monte-Carlo solution of stochastic Lagrangian drift-diffusion models coupled with Eulerian discontinuous spectral element method, Comput. Methods Appl. Mech. Eng. 384 (2021), p. 114001.
- [15] Nik M.B., Yilmaz S.L., Givi P., Sheikhi M.R.H., and Pope S.B., Simulation of Sandia Flame D using velocity-scalar filtered density function, AIAA J. 48 (2010), pp. 1513–1522.
- [16] Nik M.B., Yilmaz S.L., Sheikhi M.R.H., and Givi P., Grid resolution effects on VSFMDF/LES, Flow Turbul. Combust. 85 (2010), pp. 677–688.
- [17] Nouri A.G., Givi P., and Livescu D., Modeling and simulation of turbulent nuclear flames in type IA supernovae, Prog. Aerosp. Sci. 108 (2019), pp. 156–179.
- [18] Nouri A.G., Nik M.B., Givi P., Livescu D., and Pope S.B., Self-contained filtered density function, Phys. Rev. Fluids 2 (2017), p. 094603.
- [19] Nouri A.G., Sammak S., Pisciuneri P.H., and Givi P., Langevin simulation of turbulent combustion, in Combustion for Power Generation and Transportation, A.K. Agarwal, S. De, A. Pandey, and A.P. Singh, eds., Chap. 3, Springer, Singapore, 2017, pp. 39–53.
- [20] Pisciuneri P.H., Yilmaz S.L., Strakey P.A., and Givi P., An irregularly portioned FDF simulator, SIAM J. Sci. Comput. 35 (2013), pp. C438–C452.
- [21] Sammak S., Aitzhan A., Givi P., and Madnia C.K., High fidelity spectral-FDF-LES of turbulent scalar mixing, Combust. Sci. Technol. 192 (2020), pp. 1219–1232.
- [22] Sammak S., Brazell M.J., Givi P., and Mavriplis D.J., A hybrid DG-Monte Carlo FDF simulator, Comput. Fluids 140 (2016), pp. 158–166.
- [23] Sammak S., Nouri A.G., Brazell M.J., Mavriplis D.J., and Givi P., Discontinuous Galerkin-Monte Carlo solver for large Eddy simulation of compressible turbulent flows, in 55th AIAA Aerospace Sciences Meeting, AIAA, Grapevine, TA, 2017, p. 0982.
- [24] Sewerin F. and Rigopoulos S., An LES-PBE-PDF approach for predicting the soot particle size distribution in turbulent flames, Combust. Flame 189 (2018), pp. 62–76.
- [25] Turkeri H., Pope S.B., and Muradoglu M., A LES/PDF simulator on block-structured meshes, Combust. Theory Model. 23 (2019), pp. 1–41.
- [26] Turkeri H., Zhao X., Pope S.B., and Muradoglu M., Large eddy simulation/probability density function simulations of the Cambridge turbulent stratified flame series, Combust. Flame 199 (2019), pp. 24–45.
- [27] Yilmaz S.L., Nik M.B., Sheikhi M.R.H., Strakey P.A., and Givi P., An irregularly portioned Lagrangian Monte Carlo method for turbulent flow simulation, J. Sci. Comput. 47 (2011), pp. 109–125.
- [28] Zhang L., Liang J., Sun M., Wang H., and Yang Y., An energy-consistency-preserving large eddy simulation-scalar filtered mass density function (LES-SFMDF) method for high-speed flows, Combust. Theor. Model. 22 (2018), pp. 1–37.
- [29] Zhou H., Yang T., and Ren Z., Differential diffusion modeling in LES/FDF simulations of turbulent flames, AIAA J. 57 (2019), pp. 3206–3212.
- [30] Chibbaro S., Marchioli C., Salvetti M.V., and Soldati A., Particle tracking in LES flow fields: Conditional Lagrangian statistics of filtering error, J. Turbul. 15 (2014), pp. 22–33.
- [31] Ge Y., Cleary M.J., and Klimenko A.Y., A comparative study of Sandia Flame series (D-F) using sparse-Lagrangian MMC modelling, Proc. Combust. Inst. 34 (2013), pp. 1325–1332.
- [32] Klimenko A.Y. and Cleary M.J., Convergence to a model in sparse-Lagrangian FDF simulations, Flow Turbul. Combust. 85 (2010), pp. 567–591.
- [33] Tirunagari R.R. and Pope S.B., LES/PDF for premixed combustion in the DNS limit, Combust. Theor. Model. 20 (2016), pp. 834–865.
- [34] Zhao X., Kolla H., Zhang P., Wu B., Calello S., and Najm H.N., *A transported probability density function method to propagate chemistry uncertainty in reacting flow CFD*, in 57th AIAA Aerospace Sciences Meeting, January 7–11, AIAA, San Diego, CA, 2019, pp. 1–12.
- [35] Zhou H., Li S., Ren Z., and Rowinski D.H., Investigation of mixing model performance in transported PDF calculations of turbulent lean premixed jet flames through Lagrangian statistics and sensitivity analysis, Combust. Flame 181 (2017), pp. 136–148.
- [36] Sammak S., Ren Z., and Givi P., Modern developments in filtered density function, in Modeling and Simulation of Turbulent Mixing and Reaction: For Power, Energy and Flight, D. Livescu, A.G. Nouri, F. Battaglia, and P. Givi, eds., Springer Singapore, Singapore, 2020, pp. 181–200.

- [37] Yang T., Yin Y., Zhou H., and Ren Z., Review of Lagrangian stochastic models for turbulent combustion, Acta Mech. Sin. 37 (2021), p. 1349.
- [38] Nonaka A., Day M.S., and Bell J.B., A conservative, thermodynamically consistent numerical approach for low mach number combustion. Part I: Single-level integration, Combust. Theor. Model. 22 (2018), pp. 156–184.
- [39] Ansari N., Jaberi F.A., Sheikhi M.R.H., and Givi P., Filtered density function as a modern CFD tool, in Engineering Applications of Computational Fluid Dynamics: Volume 1, A.R.S. Maher, ed., Chap. 1, International Energy and Environment Foundation, Najaf, 2011, pp. 1–22.
- [40] Bell J., AMR for low Mach number reacting flow, in Adaptive Mesh Refinement Theory and Applications, T. Plewa, T. Linde, and V. Gregory Weirs, eds., Springer, Berlin, Heidelberg, 2005, pp. 203–221.
- [41] Zhang W., Almgren A., Beckner V., Bell J., Blaschke J., Chan C., Day M., Friesen B., Gott K., Graves D., Katz M., Myers A., Nguyen T., Nonaka A., Rosso M., Williams S., and Zingale M., AMReX: A framework for block-structured adaptive mesh refinement, J. Open Source Softw. 4 (2019), p. 1370.
- [42] Zhang W., Almgren A., Day M., Nguyen T., Shalf J., and Unat D., BoxLib with tiling: An adaptive mesh refinement software framework, SIAM J. Sci. Comput. 38 (2016), pp. S156–S172.
- [43] Almgren A.S., Bell J.B., Colella P., Howell L.H., and Welcome M.L., A conservative adaptive projection method for the variable density incompressible Navier–Stokes equations, J. Comput. Phys. 142 (1998), pp. 1–46.
- [44] Bell J.B., Day M.S., Almgren A.S., Lijewski M.J., and Rendleman C.A., A parallel adaptive projection method for low mach number flows, Int. J. Numer. Meth. Fl 40 (2002), pp. 209–216.
- [45] Pember R.B., Howell L.H., Bell J.B., Colella P., Crutchfield W.Y., Fiveland W.A., and Jessee J.P., An adaptive projection method for unsteady, low-mach number combustion, Combust. Sci. Technol.140 (1998), pp. 123–168.
- [46] Esclapez L., Ricchiuti V., Bell J.B., and Day M.S., A spectral deferred correction strategy for low Mach number reacting flows subject to electric fields, Combust. Theor. Model. 24 (2020), pp. 194–220.
- [47] Hamon F.P., Day M.S., and Minion M.L., Concurrent implicit spectral deferred correction scheme for low-Mach number combustion with detailed chemistry, Combust. Theor. Model. 23 (2019), pp. 279–309.
- [48] Nonaka A., Bell J.B., Day M.S., Gilet C., Almgren A.S., and Minion M.L., A deferred correction coupling strategy for low mach number flow with complex chemistry, Combust. Theor. Model. 16 (2012), pp. 1053–1088.
- [49] Pazner W.E., Nonaka A., Bell J.B., Day M.S., and Minion M.L., A high-order spectral deferred correction strategy for low mach number flow with complex chemistry, Combust. Theor. Model. 20 (2016), pp. 521–547.
- [50] Dragojlovic Z., Najmabadi F., and Day M., An embedded boundary method for viscous, conducting compressible flow, J. Comput. Phys. 216 (2006), pp. 37–51.
- [51] Pember R., Almgren A., Crutchfield W., Howell L., Bell J., Colella P., and Beckner V., An embedded boundary method for the modeling of unsteady combustion in an industrial gas-fired furnace, in Fall Meeting of the Western States Section of the Combustion Institute, Combustion Institute, Stanford, CA, 1995, p. 10. https://www.osti.gov/biblio/195764.
- [52] Aspden A., Day M., and Bell J., Three-dimensional direct numerical simulation of turbulent lean premixed methane combustion with detailed kinetics, Combust. Flame 166 (2016), pp. 266–283.
- [53] Aspden A.J., Day M.S., and Bell J.B., Towards the distributed burning regime in turbulent premixed flames, J. Fluid Mech. 871 (2019), pp. 1–21.
- [54] Dasgupta D., Sun W., Day M., Aspden A.J., and Lieuwen T., Analysis of chemical pathways and flame structure for n-dodecane/air turbulent premixed flames, Combust. Flame 207 (2019), pp. 36–50.
- [55] Dasgupta D., Sun W., Day M., and Lieuwen T., Effect of turbulence-chemistry interactions on chemical pathways for turbulent hydrogen-air premixed flames, Combust. Flame 176 (2017), pp. 191–201.
- [56] Wimer N.T., Day M.S., Lapointe C., Meehan M.A., Makowiecki A.S., Glusman J.F., Daily J.W., Rieker G.B., and Hamlington P.E., Numerical simulations of buoyancy-driven flows using

- adaptive mesh refinement: Structure and dynamics of a large-scale helium plume, Theor. Comp. Fluid Dyn. 35 (2021), pp. 61–91.
- [57] Madnia C.K., Jaberi F.A., and Givi P., Large eddy simulation of heat and mass transport in turbulent flows, in Handbook of Numerical Heat Transfer, W.J. Minkowycz, E.M. Sparrow, and J.Y. Murthy, eds., 2nd ed., Chap. 5, John Wiley & Sons, Inc., New York, 2006, pp. 167–190.
- [58] Williams F.A., Turbulent combustion, in The Mathematics of Combustion, J.D. Buckmaster, ed., Chap. 3, Frontiers in Applied Mathematics, SIAM, Philadelphia, PA, 1985, pp. 97–131.
- [59] Garnier E., Adams N., and Sagaut P., Large Eddy Simulation for Compressible Flows, Springer Science & Business Media, Dordrecht, 2009.
- [60] Smagorinsky J., General circulation experiments with the primitive equations. I. The basic experiment, Mon. Weather Rev. 91 (1963), pp. 99–164.
- [61] Vreman A.W., An eddy-viscosity subgrid-scale model for turbulent shear flow: Algebraic theory and applications, Phys. Fluids 16 (2004), pp. 3670–3681.
- [62] O'Brien E.E., The probability density function (PDF) approach to reacting turbulent flows, in Turbulent Reacting Flows, P. Libby and F. Williams, eds., Topics in Applied Physics Vol. 44, Chap. 5, Springer, Heidelberg, 1980, pp. 185–218.
- [63] Williams S., Lijewski M., Almgren A., Straalen B.V., Carson E., Knight N., and Demmel J., s-Step Krylov subspace methods as bottom solvers for geometric multigrid, in 2014 IEEE 28th International Parallel and Distributed Processing Symposium, IEEE, Phoenix, AZ, 2014, pp. 1149–1158.
- [64] Musser J., Almgren A.S., Fullmer W.D., Antepara O., Bell J.B., Blaschke J., Gott K., Myers A., Porcu R., Rangarajan D., Rosso M., Zhang W., and Syamlal M., MFIX-Exa: A path toward exascale CFD-DEM simulations, Int. J. High Perform. C. 36 (2021), pp. 40–58.
- [65] Day M.S. and Bell J.B., Numerical simulation of laminar reacting flows with complex chemistry, Combust. Theor. Model. 4 (2000), pp. 535–556.
- [66] Kloeden P.E., Platen E., and Schurz H., Numerical Solution of Stochastic Differential Equations Through Computer Experiments, 1st ed., Springer-Verlag, New York, 1994.
- [67] Zhang Y. and Haworth D., A general mass consistency algorithm for hybrid particle/finite-volume PDF methods, J. Comput. Phys. 194 (2004), pp. 156–193.
- [68] Turkeri H., A general purpose large-eddy simulation/probability density function simulator on block structured grids, Ph.D. diss., Koç University, Istanbul, Turkey, 2017.
- [69] Hawkes E.R., Sankaran R., Sutherland J.C., and Chen J.H., Scalar mixing in direct numerical simulations of temporally evolving plane jet flames with skeletal CO/H₂ kinetics, Proc. Combust. Inst. 31 (2007), pp. 1633–1640.
- [70] Punati N., Sutherland J.C., Kerstein A.R., Hawkes E.R., and Chen J.H., An evaluation of the one-dimensional turbulence model: Comparison with direct numerical simulations of CO/H₂ jets with extinction and reignition, Proc. Combust. Inst. 33 (2011), pp. 1515–1522.
- [71] Sen B.A., Hawkes E.R., and Menon S., Large eddy simulation of extinction and reignition with artificial neural networks based chemical kinetics, Combust. Flame 157 (2010), pp. 566–578.
- [72] Vo S., Kronenburg A., Stein O.T., and Cleary M.J., MMC-LES of a syngas mixing layer using an anisotropic mixing time scale model, Combust. Flame 189 (2018), pp. 311–314.
- [73] Vo S., Stein O.T., Kronenburg A., and Cleary M.J., Assessment of mixing time scales for a sparse particle method, Combust. Flame 179 (2017), pp. 280–299.
- [74] Yang S., Ranjan R., Yang V., Sun W., and Menon S., Sensitivity of predictions to chemical kinetics models in a temporally evolving turbulent non-premixed flame, Combust. Flame 183 (2017), pp. 224–241.
- [75] Yang Y., Wang H., Pope S.B., and Chen J.H., Large-eddy simulation/probability density function modeling of a non-premixed CO/H₂ temporally evolving jet flame, Proc. Combust. Inst. 34 (2013), pp. 1241–1249.
- [76] Germano M., A statistical formulation of dynamic model, Phys. Fluids 8 (1996), pp. 565–570.
- [77] Vaghefi N.S., Nik M.B., Pisciuneri P.H., and Madnia C.K., *A Priori* assessment of the subgrid scale viscous/scalar dissipation closures in compressible turbulence, J. Turbul. 14 (2013), pp. 43–61.
- [78] Bilger R.W., The structure of diffusion flames, Combust. Sci. Technol. 13 (1976), pp. 155–170.
- [79] Peters N., Turbulent combustion, Cambridge University Press, Cambridge, 2000.
- [80] Sheikhi M.R.H., Givi P., and Pope S.B., Velocity-scalar filtered mass density function for large eddy simulation of turbulent reacting flows, Phys. Fluids 19 (2007), p. 095106.

- [81] Givi P., Jou W.H., and Metcalfe R., Flame extinction in a temporally developing mixing layer, Symp. (Int.) Combust. 21 (1986), pp. 1251–1261.
- [82] Hawkes E., Sankaran R., and Chen J., Reignition dynamics in massively parallel direct numerical simulations of CO/H₂ jet flames, in 16th Australasian Fluid Mechanics Conference. School of Engineering, The University of Queensland, Gold Coast, 2007. https://people.eng.unimelb.edu.au/imarusic/proceedings/16/Hawkes.pdf.
- [83] Hawthorne W.R., Weddell D.S., and Hottel H.C., Mixing and combustion in turbulent gas jets, Third Symp. Combustion Flame, Explosion Phenomena 3 (1948), pp. 266–288.
- [84] Givi P., Model-free simulations of turbulent reactive flows, Prog. Energy Combust. Sci. 15 (1989), pp. 1–107.
- [85] Givi P., Filtered density function for subgrid scale modeling of turbulent combustion, AIAA J. 44 (2006), pp. 16–23.
- [86] Haworth D.C., Progress in probability density function methods for turbulent reacting flows, Prog. Energy Combust. Sci. 36 (2010), pp. 168–259.
- [87] Miller R.S. and Foster J.W., Survey of turbulent combustion models for large eddy simulations of propulsive flowfields, AIAA J. 54 (2016), pp. 2930–2946.
- [88] Pope S.B., Small scales, many species and the manifold challenges of turbulent combustion, Proc. Combust. Inst. 34 (2013), pp. 1–31.
- [89] Gicquel L.Y.M., Givi P., Jaberi F.A., and Pope S.B., Velocity filtered density function for large eddy simulation of turbulent flows, Phys. Fluids 14 (2002), pp. 1196–1213.
- [90] Sheikhi M.R.H., Drozda T.G., Givi P., and Pope S.B., Velocity-scalar filtered density function for large eddy simulation of turbulent flows, Phys. Fluids 15 (2003), pp. 2321–2337.
- [91] Sheikhi M.R.H., Givi P., and Pope S.B., Frequency-velocity-scalar filtered mass density function for large eddy simulation of turbulent flows, Phys. Fluids 21 (2009), p. 075102.
- [92] Klimenko A.Y., Lagrangian particles with mixing. II. Sparse-Lagrangian methods in application for turbulent reacting flows, Phys. Fluids 21 (2009), p. 065102.
- [93] Wang H., Popov P.P., and Pope S.B., Weak second-order splitting schemes for Lagrangian Monte Carlo particle methods for the composition PDF/FDF transport equations, J. Comput. Phys. 229 (2010), pp. 1852–1878.
- [94] Popov P.P. and Pope S.B., Implicit and explicit schemes for mass consistency preservation in hybrid particle/finite-volume algorithms for turbulent reactive flows, J. Comput. Phys. 257 (2014), pp. 352–373.
- [95] Sitaraman H., Yellapantula S., Henry de Frahan M.T., Perry B., Rood J., Grout R., and Day M., Adaptive mesh based combustion simulations of direct fuel injection effects in a supersonic cavity flame-holder, Combust. Flame 232 (2021), p. 111531.
- [96] Drozda T.G., Sheikhi M.R.H., Madnia C.K., and Givi P., Developments in formulation and application of the filtered density function, Flow Turbul. Combust. 78 (2007), pp. 35–67.